IEEE Access
Multidisciplinary ⋮ Rapid Review ⋮ Open Access Journal

Received 20 September 2023, accepted 25 September 2023, date of publication 27 September 2023,
date of current version 4 October 2023.

Digital Object Identifier 10.1109/ACCESS.2023.3319951

RESEARCH ARTICLE

An Approach for Estimating the Cogging Torque Performance Considering Manufacturing Uncertainties for the IPM Machine

YONGXI YANG[1], WILLIAM CAI[1], XIN JIN[2], SHUO ZHANG[3], (Member, IEEE), CHENGNING ZHANG[3], RUI LI[4], AND YUE ZHAO[3]

[1]Department of Electrical Engineering, Harbin University of Science and Technology, Harbin 150080, China
[2]Beijing Institute of Space Launch Technology, Beijing 100076, China
[3]School of Mechanical and Vehicle Engineering, Beijing Institute of Technology, Beijing 100081, China
[4]Harbin Electric Corporation Jiamusi Electric Machine Company Ltd., Jiamusi 154002, China

Corresponding author: Yue Zhao (zhao_y2020@126.com)

This work was supported in part by the National Natural Science Foundation of China under Grant U21A20145, and in part by the Postdoctoral funding of Heilongjiang Province under Grant LBH-Z21064.

ABSTRACT The design tolerances and material defects are frequently inevitable in the real manufacturing process, where unexpected additional cogging torque might be caused as a result. An approach fast estimating the design performances under manufacturing uncertainties is highly expected. In this paper, the previously proposed worst-uncertain-combination-analysis (WUCA) approach is further modified, where the influences of rotor geometries could be taken into account. A 10-pole-12-slot (10P12S) permanent magnet (PM) machine with non-uniform air-gap considering the rotor uncertainties is taken as an example. The cogging torque robustness for designs with different air-gap saliency ratios are discussed and compared. A medium value of air-gap saliency is suggested to achieve a balance between the ideal and worst-scenario performance under rotor uncertainties. Three prototypes with different air-gap saliency ratios are manufactured, where the possibly worst-case under uncertainties are imitated with a special PM assembling sequence. The deduction is then verified by the experimental results of the prototypes.

INDEX TERMS Cogging torque robustness, robust design, non-uniform air-gap rotor, worst-uncertain-combination-analysis approach.

I. INTRODUCTION

The permanent magnet (PM) synchronous machines have been widely used in the industrial appliances, high-performance numerical control machine and electric vehicles [1]. Various techniques have been applied to improve the design performances in terms of power density, torque ripple and noise-vibration-harshness (NVH), and efficiency in the last decades. To obtain the smooth output torque and low cogging torque, many approaches could be adopted, such as step skewing, unequal tooth tip, slummy slot, and non-uniform air-gap rotor [2], [3], [4], [5].

Although these techniques could dramatically reduce the cogging torque in theory, none of the techniques could eliminate the torque variations [6]. The reason might be contributed to the effects of manufacturing uncertainties and material defects, because the cogging torque is sensitive to these factors. Various researches have been focused on the analysis of manufacturing uncertainties and material defects and their effects on the cogging torque [7], [8], [9], [10]. The influences of manufacturing uncertainties on the design performances for different types of electric machines are concerned, such as the axial flux PM machines [11], [12] and the stator-PM-flux-switching machines [13].

Aiming to search for a design scheme whose cogging torque is not fragile to the unexpected disturbs, i.e. which has high robustness of cogging torque, the robust design and optimization are becoming more and more popular [14], [15], [16]. Analysis of the design performance considering manufacturing uncertainties is the first step for robust

The associate editor coordinating the review of this manuscript and approving it for publication was Giambattista Gruosso.

design and optimization, which is frequently the most time-consuming part as well. A system level based robust optimization approach [17], [18], [19], [20], [21] could be adopted for the PM machines, where the design variables are categorized into different groups based on their sensitivities to the objectives. Consequently, the optimization with high number of variables is converted to two optimizations with low number of variables, and the computational cost is significantly reduced.

Conventionally, the influences of manufacturing uncertainties on the cogging torque are estimated by calculating and comparing many uncertain design variants featuring small deviations. The probability distribution function (PDF) [22] and cumulative distribution function (CDF) [23] could be frequently used to estimate the design performance. The design for the six-sigma (DFSS) robust optimization approach [14] is based on the six-sigma level of the PDF. In [23], the CDF of cogging torque performance considering manufacturing tolerances was estimated by the Dvoretzky-Kiefer-Wolfowitz inequality [24] and bootstrapping method, where the number of design variants required for FEA calculations could be reduced. However, even with the help of design of experiment approaches, the number of representative samples and the consequent computational time are still too large for engineering.

An approach that could fast estimate the design performances considering uncertainties is highly expected. Considering that the cogging torque could be estimated by the variation of magnetic energy, the analytical approaches [7], [10] are then modified to analyze the torque performance under manufacturing uncertainties. Thus, the harmonic orders of the additional cogging torque introduced could be estimated. Unfortunately, the accurate estimation of the magnitudes of additional cogging torque considering uncertainties is frequently not easily achieved at this moment, especially for the IPM machines.

Luckily, the possibly worst-scenario cogging torque under uncertainties are predicted with the analytical approach and the vector diagrams [25], [26], [27]. The worst-case cogging torque performance is then estimated by calculating several specific designs featuring uncertainties, rather than thousands of design variants. With this approach, the uncertainties on the dimensions and the residual flux density of PM, the dimensions of stator tooth [25], [27], rotor eccentricity [28] are possibly concerned with this approach. The sensitivities of cogging torque performance under uncertainties to the design parameters, such as the pole/slot configuration and pole-arc coefficients, are discussed in [29] and [30].

Based on the robustness index with worst-case performances under uncertainties [15], [31], the computational cost of robust optimization could be significantly reduced. Although the optimal results of the worst-case index based optimization might be a little conservative, it could provide some insights for the engineering.

In the authors' previous work [27], a worst-uncertain-combination-analysis (WUCA) method was proposed, where the equivalent magnetic motive force (MMF) excited by one PM is regarded as a rectangle. The possibly worst-case combination of uncertainties is only related to the pole/slot configurations, where the abundant features on the rotor of real electric machines could not be concerned. A modification on the WUCA approach is highly required.

The main contribution of this paper is to propose a modified WUCA approach to estimate the cogging torque performances under manufacturing uncertainties. With this approach, the abundant details on the rotor geometries could be taken into consideration. Consequently, the design robustness of different types of electric machines could be roughly compared with the analytical approach in the early design stage. This work would benefit a lot to the robust design and optimization of the real electric machine.

The upcoming sections of this paper are arranged as follows: The WUCA approach is briefly introduced in section II. A single-pole slotless-stator model is then proposed to modify the WUCA approach. In the next section, the additional cogging torque performances of designs featuring different pole-arc and non-uniform air-gap are analyzed with the modified WUCA approach. A 12-slot/10-pole (12S10P) interior PM (IPM) machine is selected as an example, and three prototypes are then designed and manufactured to verify the efficacy of the proposed approach.

II. COGGING TORQUE ANALYSIS APPROACH CONSIDERING MANUFACTURING UNCERTAINTIES

A. THE COGGING TORQUE ANALYSIS APPROACH

The cogging torque could be estimated by calculating the variation rate of the total energy stored in the air-gap [33]. In the equivalent MMF-permeance model, the open-circuit flux-density distributions $B_g(\theta_r, \theta_m)$ in the air-gap and the cogging torque could be obtained [34] through (1).

$$\begin{aligned} \Lambda_g(\theta_s, \theta_m) &= \Lambda_r(\theta_r)\Lambda_s(\theta_s) \\ B_g(\theta_r, \theta_m) &= F'_{pm}(\theta_r)\Lambda_g(\theta_s, \theta_m) = F_{pm}(\theta_r)\Lambda_s(\theta_s), \end{aligned} \tag{1}$$

where $F'_{pm}(\theta_r)$ represents the MMF excited by the PMs without consideration of the effects of stator slot-opening. $\Lambda_g(\theta_r, \theta_m)$ is the equivalent permeance in the air-gap, θ_r represents the circumferential position in the rotor reference frame, and θ_m is referred to as the rotor position.

The equivalent air-gap permeance model $\Lambda_g(\theta_s, \theta_m)$ can be divided into two components: the stator permeance model $\Lambda_s(\theta_s)$ and rotor permeance model $\Lambda_r(\theta_m)$ as shown in (1), which are determined by the stator slot effects and rotor saliency effect [35], [36]. The equivalent MMF on the rotor contour $F_{pm}(\theta_r)$ is the interaction of the PM-excited MMF $F'_{pm}(\theta_r)$ and $\Lambda_r(\theta_r)$ [37]. Consequently, the air-gap flux density $B_g(\theta_r, \theta_m)$ can be calculated by the stator permeance model $\Lambda_s(\theta_s)$ and equivalent rotor MMF $F_{pm}(\theta_r)$.

Thus, the cogging torque can be analyzed by the variation of coenergy W stored in the air-gap versus rotor position θ_m,

as follows:

$$T_{cog}(\theta_m) = -\frac{\partial W}{\partial \theta_m} = -\frac{\partial}{\partial \theta_m}\left(\frac{1}{2\mu}\int_V F_{pm}^2(\theta_r)\Lambda_s^2(\theta_s)dV\right) \tag{2}$$

B. COGGING TORQUE CONSIDERING UNCERTAINTIES

Without considering the saturation on the iron and flux leakage between the adjacent PMs, the $\Lambda_r(\theta_r)$ can be regarded as constant. Consequently, the equivalent MMF $F_{pm}^2(\theta_r)$ of the SPM machine within the pole-pitch is often approximated by a rectangle [38]. While for the IPM machine where the PMs berried in the rotor, a trapezoidal shape [39] or rectangle is frequently adopted. A rectangular shape of $F_{pm}^2(\theta_r)$ is used to simplify the analysis process, just as illustrated in Fig. 1 (b). The pole-pitch and PM width are denoted as α_p and α_0, respectively. The pole-arc coefficient is defined as $a_c = \alpha_0/\alpha_p$.

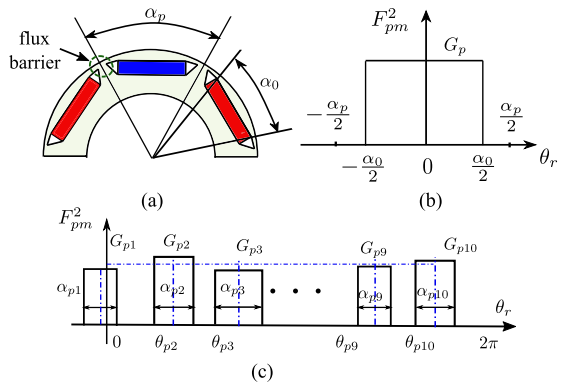

FIGURE 1. Equivalent MMF of the IPM motor. (a) Geometry of IPM rotor; (b) Equivalent F_{pm}^2 excited by one pole; (c) The equivalent F_{pm}^2 along the rotor considering the manufacturing uncertainties, where G_{pi} and α_{pi} represent the magnitude and width of the i^{th} equivalent rectangle [27].

During the real manufacturing process, uncertainties or material defects, for instance, the variations on the residual flux density B_r and dimensional defects on the PMs, are always inevitable. These uncertainties might affect the MMF excited by the PMs, and the corresponding effects could be represented by the variations of magnitude and position of rectangles of F_{pm}^2, just as illustrated in Fig. 1 (c).

C. THE WUCA APPROACH

Under imperfect manufacturing conditions, each PM might feature imperfections and the MMF magnitude can be different. In this case, the F_{pm}^2 distribution within $(0, 2\pi)$ can not directly be expressed into a Fourier series.

Luckily, the F_{pm}^2 could be regarded as the superposition of several rectangles, whose period is assumed to be infinity. Its Fourier transformation is $\mathcal{F}_d(\omega) = 2G_p \sin(\omega\alpha_0/2)/\omega$, where G_p represents the magnitude of each rectangle. The F_{pm0}^2 is then rewritten as (3), and further details are referred to the authors' previous work [27].

$$\begin{aligned} F_{pm}^2(\theta_r) &= \frac{1}{2\pi}\int_{-\infty}^{\infty}\mathcal{F}_{pm}(\omega)e^{j\omega\theta_r}d\omega \\ &= F_{pm0}^2 + \frac{1}{\pi}\sum_{n=1}^{\infty}G(n)\cos n\theta_r \\ G(n) &= \sum_{i=1}^{2p}G_d(n)e^{-jn\theta_{pi}} = \sum_{i=1}^{2p}\underbrace{\frac{2G_{pi}}{n}\sin\frac{n\alpha_{pi}}{2}}_{P_i}e^{-jn\theta_{pi}}, \end{aligned} \tag{3}$$

where $2p$ is the number of poles, $\mathcal{F}_{pm}(\omega)$ represents the fourier transformation and F_{pm0}^2 is a constant, G_{pi} and α_{pi} represent the magnitude and width of the i^{th} rectangle. The θ_{pi} corresponds to its center position, where $\theta_{pi} = 2\pi/2p\times(k-1)$ with $k = (1, 2, \ldots, 2p)$.

The $G(n)$ could be regarded as the superposition of several vectors, whose magnitudes and direction are determined by the P_i and $\varphi_i(= n\theta_{pi})$ in (3). The additional n^{th} cogging torque harmonics caused by uncertainties are mainly related to the magnitudes of $F_{pm0}^2(n)$ and $G(n)$. Consequently, the additional cogging torque harmonics due to the rotor uncertainties are the multiples of slot-number kQ_s, and those of $2pi$ orders of harmonics are frequently caused by the stator uncertainties, with k and i are integers. In this paper, only the uncertainties on the rotor aspects are concerned. Based on the typical manufacturing technique, the tolerance ranges of the PM uncertainties are listed in Table. 1.

TABLE 1. Typical value of tolerance and nominal values.

ΔB_r(T)	Δw_{pm} (mm)	Δt_m (mm)	$\Delta\theta_{pm}$ (°)
±0.03	±0.05	±0.05	±0.05

For the 12S10P machine with rotor uncertainties considered in this paper, the magnitude of $G(kQ_s)$ should be concerned. Based on the vector diagram, the $G(12)$ and $G(24)$ could be analyzed by Fig. 2. The basic value of magnitude of each vector P_0 is determined by the magnetic energy in each PM, where the residual flux density and the PM dimensions pose similar effects. The magnitudes P_i are mainly affected by the uncertainties on the PM ΔB_r and dimensions (Δt_m and Δw_{pm}), while the phase angle φ_i of each vector is influenced by the PM assembling position $n(\theta_{pi} + \Delta\theta_{pi})$.

As can be seen from Fig. 2 (a), P_1 and P_6 are the main components of $G(12)$, and vectors of PM (3, 4, 8, and 9) have negative effects on the $G(12)$. The largest value of $G(12)$ can be achieved when the sum of each vector P_i reaching the maximum value. Considering that the magnitude P_i is related to the magnetic energy in each PM, the uncertainties of (ΔB_r, Δt_m, and Δw_{pm}) would pose similar effects within the small tolerance ranges. For example, the largest P_1 can be achieved through assigning positive uncertainties on

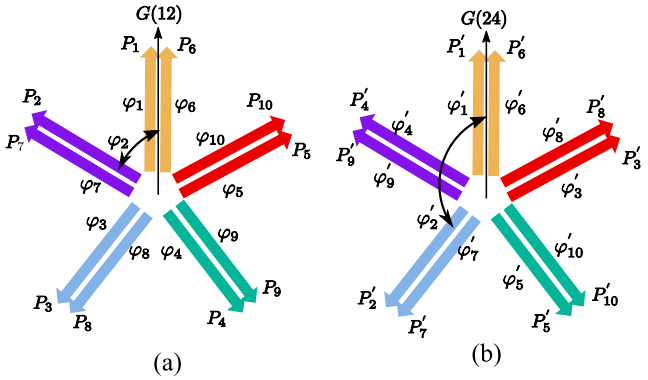

FIGURE 2. Additional 12^{th} and 24^{th} MMF harmonics caused by the uncertainties on the PMs [27].

(ΔB_r, Δt_m, and Δw_{pm}). For the uncertainties on PM 3, all of them should be with negative values. The analyzing processes for the uncertainties on other PMs are similar.

The uncertain combinations achieving the maximum $G(12)$ and $G(24)$ are reported in Table 2. Thus, the combinations of Δw_{pm} are not listed in Table 2.

TABLE 2. The possibly worst-uncertain combinations considering rotor uncertainties.

	Max $G(n=12,48)$			Max $G(n=24,36)$		
Magnet Number	(a)	(b)	(c)	(d)	(e)	(f)
1	ΔB_r	Δt_m	0	ΔB_r	Δt_m	0
2	ΔB_r	Δt_m	$-\Delta\theta_m$	$-\Delta B_r$	$-\Delta t_m$	$-\Delta\theta_m$
3	$-\Delta B_r$	$-\Delta t_m$	$-\Delta\theta_m$	ΔB_r	Δt_m	$\Delta\theta_m$
4	$-\Delta B_r$	$-\Delta t_m$	$\Delta\theta_m$	ΔB_r	Δt_m	$-\Delta\theta_m$
5	ΔB_r	Δt_m	$\Delta\theta_m$	$-\Delta B_r$	$-\Delta t_m$	$\Delta\theta_m$
6	ΔB_r	Δt_m	0	ΔB_r	Δt_m	0
7	ΔB_r	Δt_m	$-\Delta\theta_m$	$-\Delta B_r$	$-\Delta t_m$	$-\Delta\theta_m$
8	$-\Delta B_r$	$-\Delta t_m$	$-\Delta\theta_m$	ΔB_r	Δt_m	$\Delta\theta_m$
9	$-\Delta B_r$	$-\Delta t_m$	$\Delta\theta_m$	ΔB_r	Δt_m	$-\Delta\theta_m$
10	ΔB_r	Δt_m	$\Delta\theta_m$	$-\Delta B_r$	$-\Delta t_m$	$\Delta\theta_m$

The first column in the Table 2 indicates the magnet number, and columns of (a), (b), and (c) indicate the uncertainty combinations of residual flux density, width, and assemble position that results in the maximum value of $G(12)$ and $G(48)$. Similarly, columns (d)-(f) are the uncertain combinations resulting in the maximum value of $G(24)$ and $G(36)$.

With the application of the WUCA approach, the possibly worst-case considering uncertainties could be determined. The deduction was verified for various pole-slot configurations by the FEA calculations. More details are referred to as the authors' previous work [27]. The FEA calculations on only a few design schemes are required, instead of thousands, significantly reducing the calculation time.

D. APPLICATION OF THE WUCA APPROACH

With the help of the vector diagram in Fig. 2, the effects of uncertainties on the cogging torque could be analyzed through the magnitude and phase angle of vectors. The magnitude of $P_i(n)$ could be affected by the uncertainties, but it is mainly determined by the ideal-case value of $P_0(n)$.

If the MMF excited by one pole is regarded as a rectangle, the $P_0(n)$ could be written as (4). Once the term $M(n)$ in (4) can be reduced to zero with proper selection of the pole-arc coefficient a_c, the corresponding additional harmonic of $G(n)$ might be eliminated.

$$P_0(n) = \frac{2G_p}{n}\sin\frac{n\alpha_0}{2} = \frac{2G_p}{n}\underbrace{\sin\frac{na_c}{2}\frac{2\pi}{2p}}_{M(n)}. \tag{4}$$

In the conventional design practice, the pole-arc coefficient is usually selected within the range of (0.6,0.95). Once the pole/slot configuration is selected, the values of $M(n)$ for different pole-arc coefficients a_c could be determined.

The 12S10P configuration is taken as an example, and the magnitudes variation of several orders of harmonics are illustrated in Fig. 3. The main order of cogging torque harmonics of 12S10P machine is the $n = LCM(12,10)$, which is highlighted in Fig. 3. The additional kQ_s orders of cogging torque harmonics caused by the rotor uncertainties [10], [27] could be estimated by $|M(n)/n|$, where $n = kQ_s$. The higher value of $|M(n)/n|$ might indicate the relatively larger value of $G(n)$ and magnitude of n^{th} order of cogging torque.

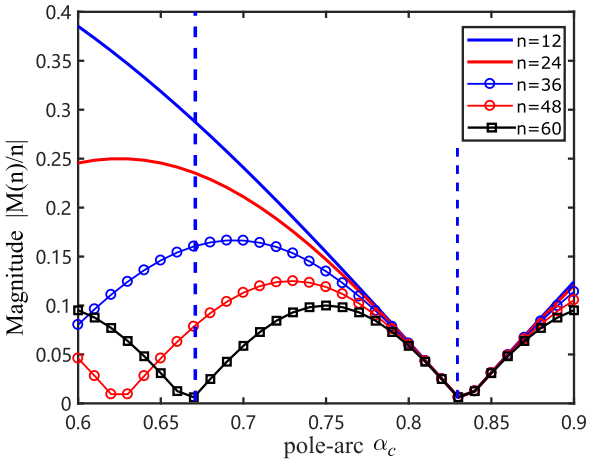

FIGURE 3. The magnitude of different harmonic orders $|M(n)|$ for various pole-arc coefficients through analytical approach.

It could be seen from Fig. 3 that $|M(12)/12|$ decreases as the pole-arc coefficients go up within the range of $a_c = (0.67, 0.83)$, which indicates the variation of additional 12^{th} cogging torque under rotor uncertainties. As for the variation of $|M(60)/60|$ within the range pole-arc, its value dramatically changes as illustrated in Fig. 3. The minimum value of $|M(60)|$ achieves when ($a_c = 0.67$) and ($a_c = 0.83$),

and this means the minimum value of $T_{cog}(60)$ would be achieved around these values of pole-arc coefficients.

E. THE SINGLE-POLE SLOTLESS-STATOR MODEL

In the real design practice, the rotor geometries are frequently complicated with non-uniform air-gap length and dummy slots to reduce the cogging torque and NVH. Besides, due to the saturation effects and flux leakages between the adjacent PMs, the PM-excited MMF is frequently not the ideal rectangular shape.

To modify the MMF in real design practice, a single-pole slotless-stator (SPS) model-based approach is proposed, where the air-gap flux density and the equivalent MMF are obtained through FEA calculations. In the SPS model, only one pole with the real rotor counter is required. Since only the PM-excited MMF is concerned in this part, the symmetrical boundary could be adopted regardless of the real pole/slot configurations. The FEA model and the corresponding results are illustrated in Fig. 4.

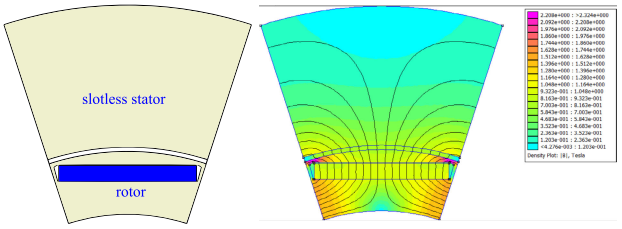

FIGURE 4. The single-pole slotless-stator model and the corresponding no-load results with FEA.

In the slotless model, the relative permeance variation due to the stator slot effect is eliminated, and the $\Lambda_s(\theta_s)$ could be regarded as a constant. The rotor MMF is mainly related to the distribution of radial component of the air-gap flux density with ($F_{pm} \propto B_g$). Consequently, the rotor MMF (F_{pm}) considering various rotor geometries and pole-arc coefficients could be taken into account.

With the adoption of the SPS model, the air-gap flux density of the design in Fig. 4 within one pole-pitch is shown in Fig. 5(a), whose shape is similar to a rectangle. The equivalent F_{pm}^2 is estimated by the distribution of air-gap flux density, where $F_{pm}^2 = AB_g^2$ with A is a constant. The calculated F_{pm}^2 is illustrated in Fig. 5(a) as well. The Fast Fourier Transform (FFT) is carried out on the calculated F_{pm}^2, and the first 70^{th} orders of harmonics are presented in Fig. 5(b).

The magnitude of each order of harmonics obtained in Fig. 5(b) could be adopted to modify the $P_i(n)$, and then further used to estimate the design performance for the ideal-case and scenarios with manufacturing uncertainties.

The main additional cogging torque harmonic orders, caused by the rotor uncertainties, are those multiplies of slot numbers. Thus, the lower orders of $12k^{th}$ of harmonics in $|M(n)|$ should be mainly concerned in this paper.

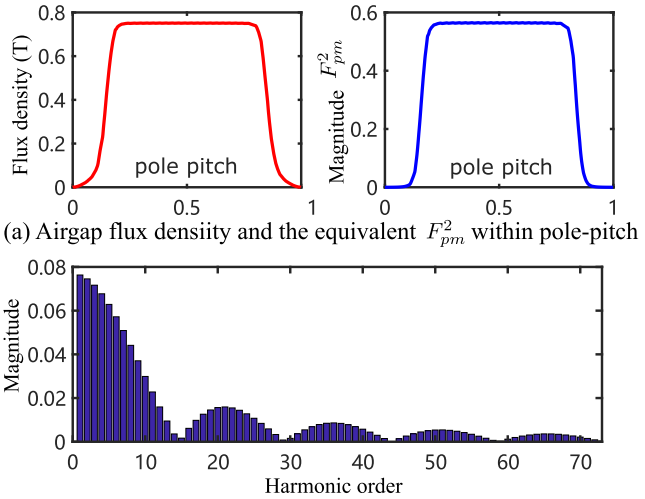

(a) Airgap flux densiity and the equivalent F_{pm}^2 within pole-pitch

(b) Harmonics of the equivalent F_{pm}^2 within the pole-pitch

FIGURE 5. The equivalent F_{pm}^2 and corresponding harmonics obtained through single-pole slotless-stator approach.

To estimate the cogging torque performances of designs featuring different a_c, several design schemes are analyzed through the SPS model-based approach. The air-gap flux density of the different designs are calculated and presented in Fig. 6. The shapes of air-gap flux densities B_{gi} are similar to rectangles, whose width and magnitudes increase with the rise of pole-arc coefficients a_c.

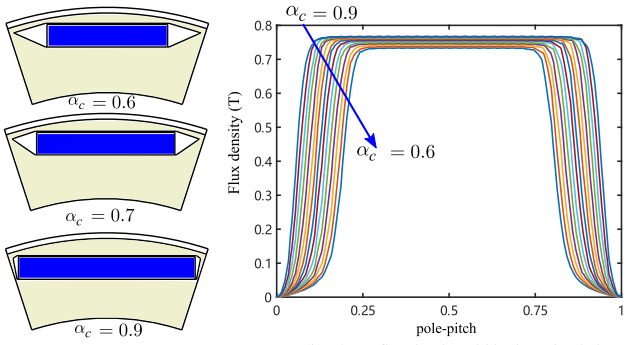

(a) Rotor with different pole-arc α_p

(b) Airgap flux density within the pole-pitch

FIGURE 6. Rotor geometries and the corresponding air-gap flux densities with various pole-arc coefficients a_c.

The equivalent F_{pm}^2 of each design is calculated and then analyzed with the FFT operation. The magnitudes of $F_{pm}^2(n)$ versus a_c are illustrated in Fig. 7. Compared with the analytical approach in Fig. 3, the variation of each order of harmonics is quite similar in these two figures, which indicates the efficacy of the analytical and SPS based approaches.

Considering the effects of flux leakages and saturation in the rotor iron, the minimum value of the n^{th} harmonics slightly vary. However, the main trend of each harmonics is quite similar in the two figures.

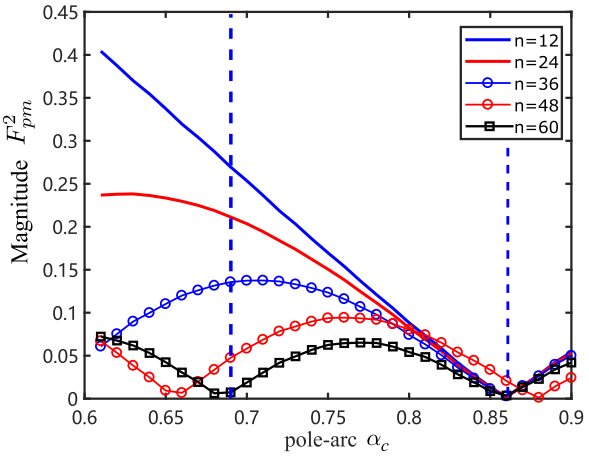

FIGURE 7. The magnitude of different harmonic orders $F_{pm}^2(n)$ versus various pole-arc coefficients a_c through the SPS based approach.

As mentioned previously, the cogging torque harmonic is related to the magnitude of the corresponding $F_{pm}^2(n)$. Thus, the 60^{th} cogging torque for designs with different pole-arc coefficients should show similar variation as that $F_{pm}^2(60)$ in Fig. 7. The cogging torque performance of 12S10P IPM machines featuring different pole-arc are then analyzed.

Several models of 12S10P IPM motor with different pole-arc coefficients a_c are built and calculated through the FEA. These models feature the same stator and rotor geometries, and the only difference is on the pole-arc coefficient a_c, which is reflected on the width dimension of the PM.

The FFT operation is then adopted to analyze the cogging torque harmonics for each design. The magnitude of the 60^{th} order of cogging torque is illustrated in Fig. 8.

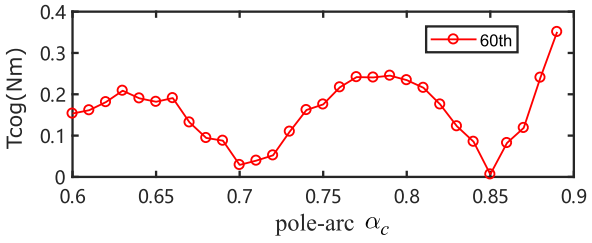

FIGURE 8. The magnitude of 60^{th} order cogging torque for 12S10P machine with different pole-arc α_c.

As can be seen from Fig. 8, the variation trend of the 60^{th} order of cogging torque is similar to that of $F_{pm}^2(60)$ in Fig. 7. The minimum value of $M(60)$ is achieved when $a_c = 0.67$ and $a_c = 0.83$ from the analytical approach of (4), while the minimum value of $F_{pm}^2(60)$ was obtained when $a_c = 0.69$ and $a_c = 0.86$ in the proposed approach. Although there are slight differences between the proposed approach and the results of real FEA calculation in Fig. 8, the basic trend and location of the a_c are similar. The differences might be contributed to effects of the saturation and flux leakages, which are not considered in the analytical and slotless model.

Thus, the 60^{th} order of cogging torque results from the magnitude of $F_{pm}^2(60)$, and both the analytical approach and the proposed slotless model could estimate the variation trend of $T_{cog}(60)$. Moreover, a rapid increase of $T_{cog}(60)$ could be observed when the a_c is larger than 0.85, and the reason might be concluded to the local saturation on the stator teeth.

F. THE MODIFIED WUCA APPROACH

In this part, the WUCA approach is then modified with the SPS model calculated MMF, instead of the ideal rectangle in previous work [27]. Even with the modified approach, the possibly worst-case cogging torque considering rotor uncertainties could be identified by the vector diagram as well. The modified WUCA approach is then applied to analyze the cogging torque performances of the ideal case and worst-case.

For the previously concerned 12S10P IPM machines, the main additional cogging torque harmonic orders are those of $12k^{th}$. The possibly worst scenarios might related to the maximum value of $G(Q_s)$ and $G(2Q_s)$, where the uncertain combinations are identified by vector diagram and Table. 2. Only the uncertainties of ΔB_r with a range of $\pm 0.03T$ is considered in this part. The two possible worst cases cogging torque are denoted as T_{w1} and T_{w2}.

A sensitivity index S_{en} is proposed to estimate the design robustness considering manufacturing uncertainties, where a lower value of S_{en} indicating higher robustness. Further details are referred to [29].

$$S_{en} = \max(T_{w1}, T_{w2}) - T_n \tag{5}$$

The ideal-case peak-to-peak cogging torque T_n of the models with different a_c are shown in Fig. 9 (a), and the sensitivity index *Sen* is presented with blue circles as well.

It can be seen from Fig. 9 that the sensitivity index *Sen* varies for different pole-arc coefficients a_c, whose trend is different from that of the ideal-case torque T_n. Taking the design A with $a_c = 0.7$ as an example, the ideal-case cogging torque is about 0.1Nm. However, the corresponding value of *Sen* is as high as 0.9Nm in the worst scenario, indicating its high sensitivity to the rotor uncertainties. The reason could be contributed to the high values of $(F_{pm}^2(n)|n = 12, 24, 36)$ when $a_c = 0.7$ in Fig. 7. On the contrary, the minimum value of $F_{pm}^2(n)$ is achieved when $(a_c = 0.85)$, where the sensitivity index *Sen* is approximately 0.2Nm.

In Fig. 9, the design *A* is better than *B* with the lower value of T_n in ideal-case, however, it is more susceptible to the manufacturing uncertainties, whose value of *Sen* is much higher. The worst-case cogging torque components of the two designs are presented in Fig. 9 (b) and (c).

As can be seen, almost all the additional $12k^{th}$ harmonics are high in design *A*, which is in consistent with the high values of $M(n)$ and $F_{pm}^2(n)$ (for *A* in Fig. 3 and Fig. 7). In the real design practice, designs like *A* with good nominal performance but highly susceptible to manufacturing uncertainties should be avoided. On the contrary, the design *B* with a lower value of $F_{pm}^2(n)$ should be recommended,

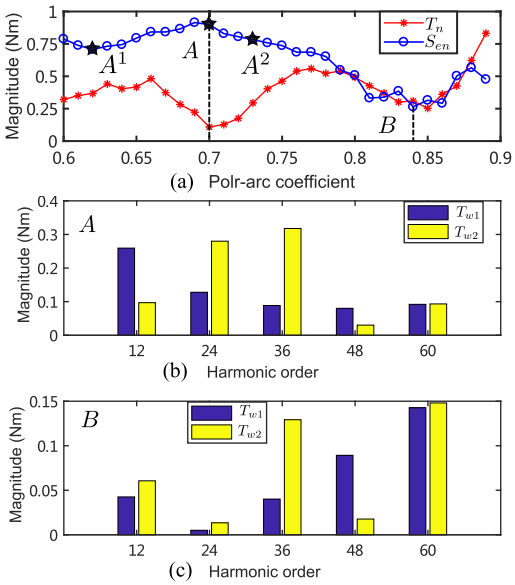

FIGURE 9. Cogging torque performance of the 12S10P IPM motor; (a) Peak-to-peak cogging torque and its sensitivity versus pole-arc coefficient; (b)-(c) Cogging torque harmonic analysis for the worst-case of design A and B under uncertainties. [29].

where good design performances of ideal-case and imperfect-case could be achieved.

III. APPLICATION OF THE MODIFIED WUCA APPROACH

In the real design application, the rotor with a non-uniform air-gap is frequently adopted. The non-uniform air-gap technique involves the inverse cosine pole shoe, center-offset arc pole shoe [32], and the eccentric arc pole shoe [40]. The third one is easy to achieve in mass production as it is consisted of two separate arcs instead of a complicated mathematical curve.

An example of rotor with the non-uniform air-gap is illustrated in Fig. 10. The saliency ratio k_{dq} is defined as the ratio of air-gap length of q-axis and d-axis, ($k_{dq} = g_q/g_d$). The rotor with uniform air-gap rotor corresponds to ($k_{dq} = 1$).

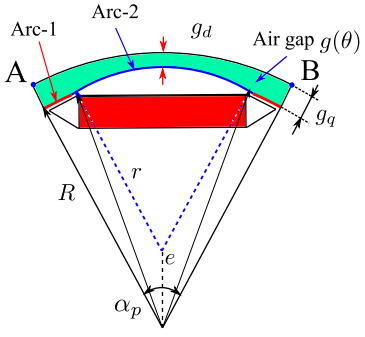

FIGURE 10. The geometry of non-uniform rotor.

The single-pole slotless model modified WUCA approach is applied on the PM machine with a non-uniform air-gap, and the cogging torque performance of designs considering manufacturing uncertainties are analyzed in this part.

A. ROTOR WITH DIFFERENT AIR-GAP SALIENCY

The rotor geometries for different k_{dq} are presented in Fig. 11 (a), where the d-axis air-gap and the PM width keeps the same. The PM-excited MMF within one pole-pitch is then calculated with the SPS approach. The distribution of radial component of air-gap flux density B_g for different k_{dq} is illustrated in Fig. 11 (b).

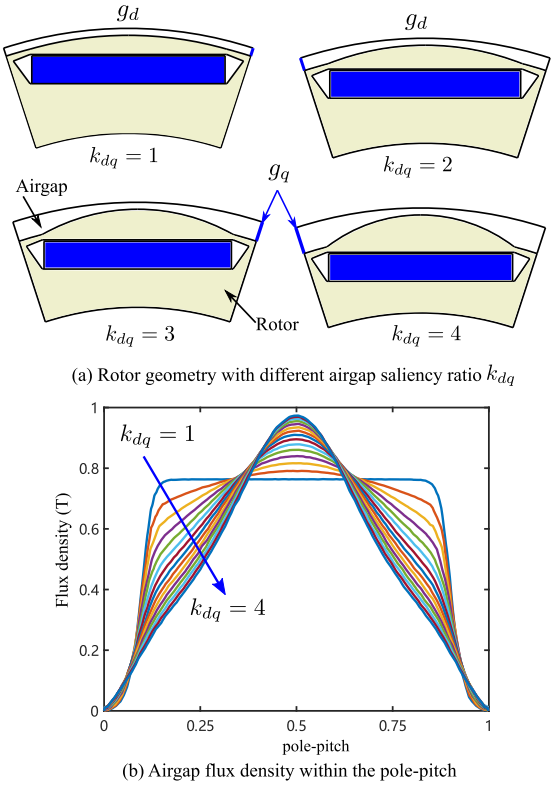

FIGURE 11. The rotor geometries and the corresponding air-gap flux density distribution within one pole-pitch for different k_{dq}.

It can be seen that the one PM excited B_g becomes relatively more sinusoidal as the air-gap saliency k_{dq} increases, and this would frequently result in a smoother cogging torque and output torque.

As mentioned in the previous section, the larger magnitudes of $F_{pm}^2(n)$ might contribute to higher cogging torque. Thus, the equivalent F_{pm}^2 within a pole-pitch is calculated based on the SPS model, and the 60^{th} order of harmonic is illustrated in Fig. 12. The cogging torque of designs featuring different k_{dq} are calculated, and the magnitudes og 60^{th} orders of harmonics are presented in Fig. 12 as well.

It could be seen from Fig. 12 that the 60^{th} cogging torque and $F_{pm}^2(60)$ show a similar trend with the variation of air-gap saliency k_{dq}. The 60^{th} order of cogging torque decrease with the k_{dq} increasing, where similar phenomenon could be observed from the SPS model based $F_{pm}^2(60)$. It is a little weird that minimum value of $T_{cog}(60)$ locates around

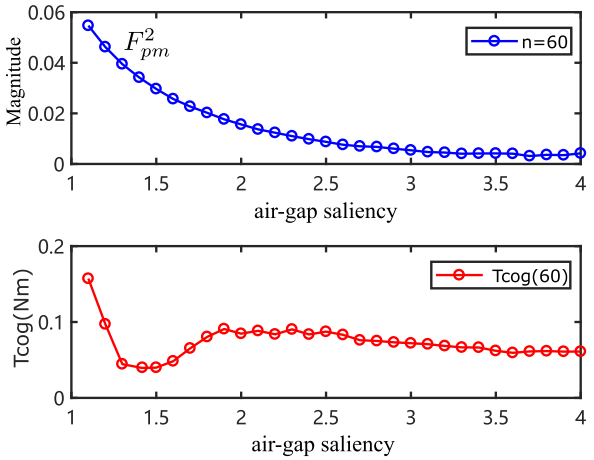

FIGURE 12. Comparison on the magnitude of cogging torque harmonics and the equivalent F_{pm}^2 for different air-gap saliency k_{dq}.

($k_{dq} = 1.5$), which is not consistent with the variation of $F_{pm}^2(60)$. The reason might be contributed to the tangential flux leakage or local saturation on the teeth for the larger air-gap saliencies.

To further analyze the design performances under the imperfection scenarios, the additional cogging torque related harmonics of kQ_s are concerned. The equivalent $F_{pm}^2(n)$ for different k_{dq} are then analyzed with FFT, and the magnitudes of $F_{pm}^2(kQ_s)$ are illustrated in Fig. 13.

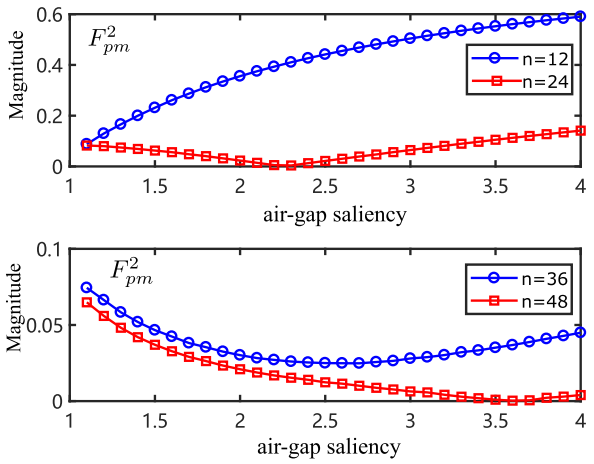

FIGURE 13. The magnitudes of harmonics for the equivalent F_{pm}^2 with different air-gap saliency k_{dq}.

The cogging torque performances of designs featuring rotor uncertainties are analyzed and calculated, where the tolerance ranges are presented in Table. 1. The possible worst-cases are estimated through the WUCA approach, and the two possibly worst uncertain combinations are as presented in Table. 2. The magnitudes of $T_{cog}(n)$ is estimated by the two possibly worst-cases under uncertainties with $T_{cog}(n) = max[T_{w1}(n), T_{w2}(n)]$. The magnitudes of cogging torque harmonics considering uncertainties for different air-gap sailency k_{dq} are then presented in Fig. 14.

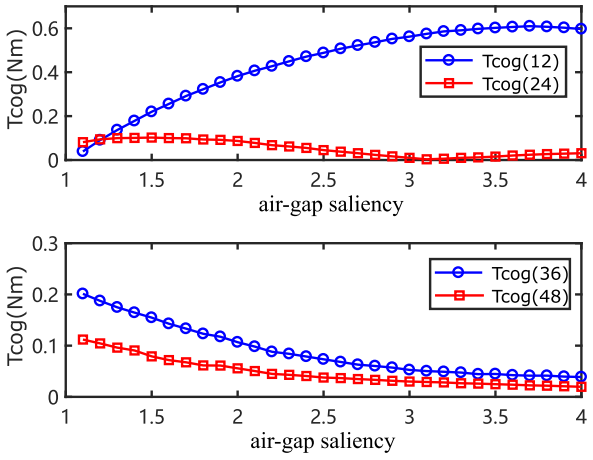

FIGURE 14. Cogging torque harmonic analysis considering uncertainties for designs featuring different k_{dq}.

The maximum 12^{th} order of cogging torque caused by the uncertainties increases with the rise of k_{dq} in Fig. 14, where a similar trend could be observed from $F_{pm}^2(12)$ in Fig. 13. Similar phenomenons could be found for the cogging torque harmonics of 24^{th} and 48^{th}.

Although the variation trend of the 36^{th} cogging torque and $F_{pm}^2(36)$ are slightly different, the main trend within the range of (1, 3) is similar. The difference might be caused by the local saturation or tangential flux leakages in the teeth.

Based on the analysis result of $F_{pm}^2(n)$ through the SPS model and Fig. 12 to Fig. 14, some deductions could be obtained. The ideal-case cogging torque decreases with the air-gap saliency k_{dq} increasing, but a minimum value might occur around ($k_{dq} = 1.5$). As the magnitude of $F_{pm}^2(12)$ is much larger than the other orders of harmonics, its effects on the cogging torque performance should be concerned. The higher value of additional $T_{cog}(12)$ might be introduced under rotor uncertainties when the rotor is large saliency.

B. COGGING TORQUE ROBUSTNESS CONSIDERING UNCERTAINTIES FOR DIFFERENT K_{DQ}

To verify the deductions, the peak-to-peak cogging torque and its sensitivity *Sen* considering rotor uncertainties are compared, as illustrated in Fig. 15.

Several designs are highlighted in Fig. 15. It can seen that the peak-to-peak cogging torque is approximately 0.5Nm for the design A (with $k_{dq} = 1$), and its sensitivity index value becomes about 0.83Nm under the worst-case uncertain combinations. As for the design E (with $k_{dq} = 3$), the nominal value T_n is 0.12Nm, but its corresponding *Sen* might achieve an extremely high value of 1.35Nm in the worst scenario.

In other words, if the design E is manufactured for mass production, the peak-to-peak cogging torque could be any value within the range of (0.12Nm, 1.47Nm), and this might not be acceptable for the manufacturers and customers.

Two design models with different air-gap saliency ratios are built and calculated by FEA. The cogging torque

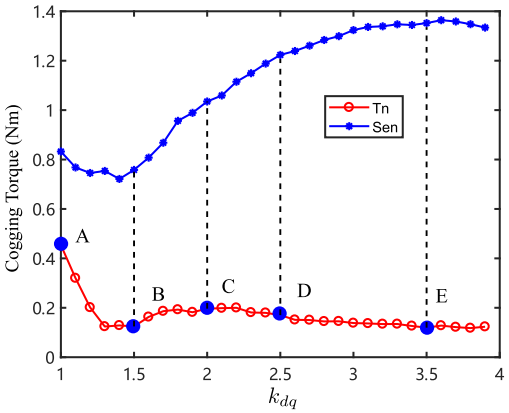

(a)The cogging torque and sensitivity vs central-arc coeffient

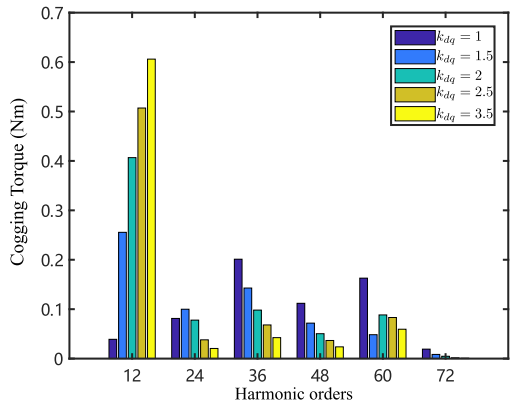

(b) Cogging Torque harmonics under the worst-case

FIGURE 15. The peak-to-peak cogging torque and the corresponding sensitivities considering rotor uncertainties for designs featuring different air-gap saliency k_{dq}.

performance of the uniform rotor (design A with $k_{dq} = 1$) and the salient rotor (design D with $k_{dq} = 2.5$) under the ideal scenario (T_n) are compared. The two possible worst-cases (T_{w1} and T_{w2}) considering PM uncertainties for the two designs are presented in Fig. 16.

As can be seen from Fig. 16 that the worst-case cogging torque for design with a higher value of k_{dq} is higher, which indicates a higher sensitivity and low robustness to the manufacturing uncertainties.

Consequently, if a robust design with low sensitivity to the rotor uncertainties is expected, a medium value of air-gap saliency k_{dq} might be recommended.

C. MOTOR PROTOTYPES AND EXPERIMENTAL VERIFICATION

A 10P12S IPM machine is taken as an example in this part. Three small prototypes with a rated power of 1.5kW are then fabricated to verify the effects of k_{dq} on the cogging torque robustness. The basic parameters of the prototypes are presented in Table. 3. The only differences among the three prototypes are the rotor saliency ratio k_{dq}. All the other parameters, such as the dimensions of the PMs and the d-axis air-gap length g_d, keep the same.

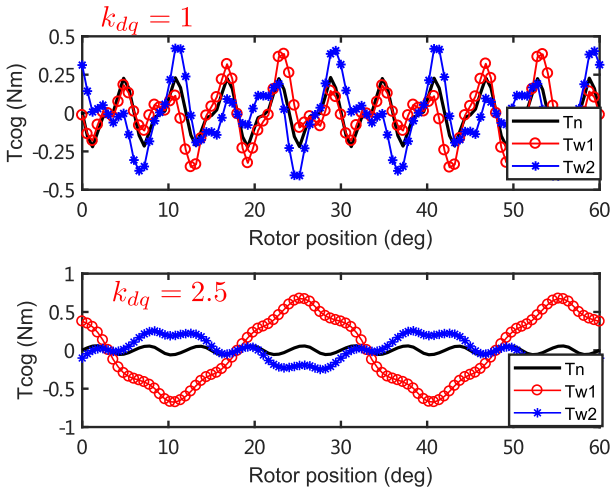

FIGURE 16. The cogging torque performance of two designs considering rotor uncertainties.

TABLE 3. Motor data of the prototypes.

Rated torque (Nm)	8	Rated speed (rpm)	1500
Airgap length (mm)	0.8	Slot opening width (mm)	4.2
Tooth width (mm)	9.3	Slot depth (mm)	22
Rotor outer diameter (mm)	58.4	Rotor inner diameter (mm)	30
PM width (mm)	12.8	PM thickness (mm)	4

Three values of the ($k_{dq} = 1, 1.4, 2.5$) are selected for fabricating the motors, and their geometries are presented in Fig. 17. The corresponding motors are then denoted as S1R1, S1R2, and S1R3 in the following parts.

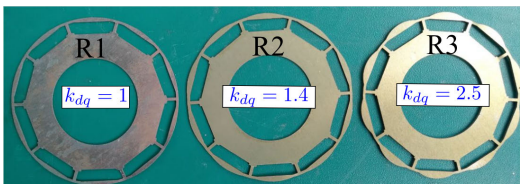

(a) (b) (c)

FIGURE 17. Three rotor geometries with different k_{dq}.

To imitate the effects of PM uncertainties under the worst scenarios, a batch of PMs are manufactured. The magnetic flux value of each PM is measured and categorized into several groups based on their variations to the ideal value. Several PMs with the maximum and minimum magnetic flux values are selected, and then assembled in a special sequence as that in Table. 2 (a) for the prototypes. Consequently, the maximum 12^{th} order of additional cogging torque would be introduced.

The cogging torque performances of the three prototypes are then measured with the test bench, as illustrated in Fig. 18. A high-performance torque transducer with KISLER measurement, whose minimum measuring accuracy is 0.1 mNm, is adopted in the test bench. The tested motor is rotated by the

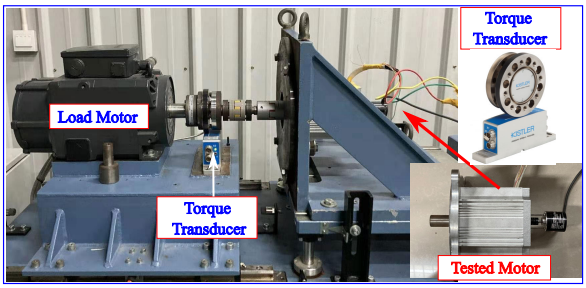

FIGURE 18. Three rotors with different k_{dq} and the test bench for cogging torque.

load motor with a rotational speed of 1rpm, and the cogging torque data is then saved and transferred to a laptop.

Considering that other types of uncertainties due to the motor assembling and testbench are inevitable, the lower order of harmonics of the test data are filtered. Only those orders of harmonics related to the rotor and stator uncertainties are remained in this work. The cogging torque performances considering the PM uncertainties for the prototypes S1R1 to S1R3 are illustrated in Fig. 19. It can be seen that the peak-to-peak value of the three motors under PM uncertainties are at a similar level. The torque harmonics of the three prototypes are analyzed through the FFT analysis.

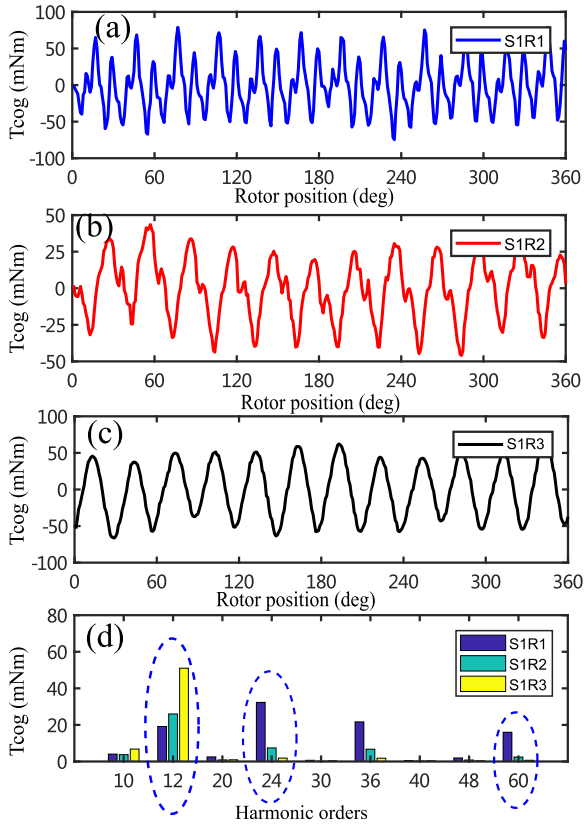

FIGURE 19. The experimental test results of the cogging torque for the three different designs. (a)-(c) are the measured cogging torque for the three designs, (d) the comparisons of the cogging torque harmonics.

The 60^{th} order of harmonics are the main components if the uncertainties on the PM are not considered. The design S1R3 with larger k_{qd} present the lowest value of 60^{th} torque harmonics, indicating its superiority in the ideal scenario.

However, a much higher value of additional $T_{cog}(12)$ could be observed in the S1R3. This indicates that the cogging torque would be much higher than the theoretically designed value in the real manufacturing process.

The measured additional cogging torque harmonics for prototypes with different k_{dq} have a similar trend with that in Fig. 15. Consequently, the effectiveness of the SPS-model modified WUCA approach could be verified.

Among these three prototypes, the design S1R2 with a small k_{dq} shows good performance under the ideal-case (60^{th} order of harmonics) and worst scenarios (additional $12k^{th}$ orders), and this makes it a good option for mass production where the manufacturing uncertainties are inevitable.

IV. CONCLUSION

In this paper, the previously proposed worst-uncertain-combination-analysis approach (WUCA) is further modified, where the details on the rotor geometries could be taken into account. The proposed approach is applied to estimate the cogging torque performance of IPM machine with different rotors. The results are verified with both the FEA calculations and the experimental tests of the prototypes. Some conclusions could be obtained in the following.

(1) A single-pole slotless-stator (SPSS) model based on the FEA is proposed to modify the WUCA approach, where the effects of the real rotor geometries could be taken into account. The analysis result of the additional cogging torque based on the rectangular MMF shows a similar trend with the modified approach, indicating the efficacy of the two approaches.

(2) With the proposed approach, the worst scenario cogging torque performances for rotors with different pole-arc coefficients a_c and rotor saliencies k_{dq} could be fast estimated and compared.

(3) The cogging torque sensitivity of designs with various a_c could be different. The design with low nominal value of T_{cog} might show higher sensitivity to manufacturing uncertainties, and the robustness evaluation is critical/

(4) Although the lower cogging torque can be theoretically obtained with a large k_{dq}, the introduced lower orders of additional cogging torque might not be ignored when the manufacturing uncertainties are involved. A medium value of air-gap saliency is suggested to achieve a balance between the ideal and worst scenario performances.

REFERENCES

[1] K. T. Chau, C. C. Chan, and C. Liu, "Overview of permanent-magnet brushless drives for electric and hybrid electric vehicles," *IEEE Trans. Ind. Electron.*, vol. 55, no. 6, pp. 2246–2257, Jun. 2008.

[2] N. Bianchi and S. Bolognani, "Design techniques for reducing the cogging torque in surface-mounted PM motors," *IEEE Trans. Ind. Appl.*, vol. 38, no. 5, pp. 1259–1265, Sep./Oct. 2002.

[3] T. A. Anuja, M. A. N. Doss, R. Senthilkumar, K. S. Rajesh, and R. Brindha, "Modification of pole pitch and pole arc in rotor magnets for cogging torque reduction in BLDC motor," *IEEE Access*, vol. 10, pp. 116709–116722, 2022.

[4] H. Huang, D. Li, X. Ren, and R. Qu, "Analysis and reduction methods of cogging torque in dual PM Vernier machines with unevenly distributed split teeth," *IEEE Trans. Ind. Appl.*, vol. 58, no. 4, pp. 4637–4647, Jul. 2022.

[5] L. Wu, H. Chen, T. Yu, C. Sun, L. Wang, X. Ye, and G. Zhai, "Robust design optimization of the cogging torque for a PMSM based on manufacturing uncertainties analysis and approximate modeling," *Energies*, vol. 16, no. 2, p. 663, Jan. 2023.

[6] G. Bramerdorfer, J. A. Tapia, J. J. Pyrhönen, and A. Cavagnino, "Modern electrical machine design optimization: Techniques, trends, and best practices," *IEEE Trans. Ind. Electron.*, vol. 65, no. 10, pp. 7672–7684, Oct. 2018.

[7] L. Gasparin, A. Cernigoj, S. Markic, and R. Fiser, "Additional cogging torque components in permanent-magnet motors due to manufacturing imperfections," *IEEE Trans. Magn.*, vol. 45, no. 3, pp. 1210–1213, Mar. 2009.

[8] M. A. Khan, I. Husain, M. R. Islam, and J. T. Klass, "Design of experiments to address manufacturing tolerances and process variations influencing cogging torque and back EMF in the mass production of the permanent-magnet synchronous motors," *IEEE Trans. Ind. Appl.*, vol. 50, no. 1, pp. 346–355, Jan. 2014.

[9] X. Ge and Z. Q. Zhu, "Influence of manufacturing tolerances on cogging torque in interior permanent magnet machines with eccentric and sinusoidal rotor contours," *IEEE Trans. Ind. Appl.*, vol. 53, no. 4, pp. 3568–3578, Jul. 2017.

[10] J. Ou, Y. Liu, R. Qu, and M. Doppelbauer, "Experimental and theoretical research on cogging torque of PM synchronous motors considering manufacturing tolerances," *IEEE Trans. Ind. Electron.*, vol. 65, no. 5, pp. 3772–3783, May 2018.

[11] A. Escobar, G. Sánchez, W. Jara, C. Madariaga, J. Tapia, M. Degano, and J. Riedemann, "Statistical analysis of manufacturing tolerances effect on axial-flux permanent magnet machines cogging torque," in *Proc. IEEE Energy Convers. Congr. Expo. (ECCE)*, Oct. 2021, pp. 4342–4346.

[12] A. Escobar, C. Madariaga, W. Jara, J. A. Tapia, M. Degano, and J. Riedemann, "Continuous-domain semi-analytical method for tolerance analysis of axial flux permanent magnet machines," in *Proc. IEEE Energy Convers. Congr. Expo. (ECCE)*, Oct. 2022, pp. 1–6.

[13] Z. Zhang, W. Hua, P. Wang, W. Yu, M. Hu, G. Zhang, and M. Cheng, "Torque characteristics of SPM-FS machines with functional-contour salient pole rotors considering manufacturing error," *IEEE Trans. Energy Convers.*, vol. 37, no. 4, pp. 2645–2656, Dec. 2022.

[14] B. Ma, G. Lei, J. Zhu, Y. Guo, and C. Liu, "Application-oriented robust design optimization method for batch production of permanent-magnet motors," *IEEE Trans. Ind. Electron.*, vol. 65, no. 2, pp. 1728–1739, Feb. 2018.

[15] Y. Yang, N. Bianchi, G. Bacco, S. Zhang, and C. Zhang, "Methods to reduce the computational burden of robust optimization for permanent magnet motors," *IEEE Trans. Energy Convers.*, vol. 35, no. 4, pp. 2116–2128, Dec. 2020.

[16] S. Kim, S.-G. Lee, J.-M. Kim, T. H. Lee, and M.-S. Lim, "Robust design optimization of surface-mounted permanent magnet synchronous motor using uncertainty characterization by bootstrap method," *IEEE Trans. Energy Convers.*, vol. 35, no. 4, pp. 2056–2065, Dec. 2020.

[17] G. Lei, T. Wang, J. Zhu, Y. Guo, and S. Wang, "System-level design optimization method for electrical drive systems—Robust approach," *IEEE Trans. Ind. Electron.*, vol. 62, no. 8, pp. 4702–4713, Aug. 2015.

[18] G. Lei, J. Zhu, Y. Guo, C. Liu, and B. Ma, "A review of design optimization methods for electrical machines," *Energies*, vol. 10, no. 12, p. 1962, Nov. 2017.

[19] K. Diao, X. Sun, G. Lei, G. Bramerdorfer, Y. Guo, and J. Zhu, "System-level robust design optimization of a switched reluctance motor drive system considering multiple driving cycles," *IEEE Trans. Energy Convers.*, vol. 36, no. 1, pp. 348–357, Mar. 2021.

[20] J. Wu, X. Zhu, Z. Xiang, D. Fan, L. Quan, and L. Xu, "Robust optimization of a rare-earth-reduced high-torque-density PM motor for electric vehicles based on parameter sensitivity region," *IEEE Trans. Veh. Technol.*, vol. 71, no. 10, pp. 10269–10279, Oct. 2022.

[21] Y. Cheng, L. Ding, T. Zhao, and S. Cu, "Design and optimization of electric vehicle traction motor considering rotor topology and manufacturing uncertainty," *IEEE Trans. Ind. Electron.*, early access, Jun. 26, 2023, doi: 10.1109/TIE.2023.3288195.

[22] M. Katona, M. Kuczmann, and T. Orosz, "Accuracy of the robust design analysis for the flux barrier modelling of an interior permanent magnet synchronous motor," *J. Comput. Appl. Math.*, vol. 429, Sep. 2023, Art. no. 115228.

[23] E. Marth and G. Bramerdorfer, "On the use of the cumulative distribution function for large-scale tolerance analyses applied to electric machine design," *Stats*, vol. 3, no. 3, pp. 412–426, Sep. 2020.

[24] L. Wasserman, *All of Statistics: A Concise Course in Statistical Inference*, vol. 26. Cham, Switzerland: Springer, 2004.

[25] X. Ge and Z. Q. Zhu, "Sensitivity of manufacturing tolerances on cogging torque in interior permanent magnet machines with different slot/pole number combinations," *IEEE Trans. Ind. Appl.*, vol. 53, no. 4, pp. 3557–3567, Jul. 2017.

[26] M. Nakano, Y. Morita, and T. Matsunaga, "Reduction of cogging torque due to production tolerances of rotor by using dummy slots placed partially in axial direction," *IEEE Trans. Ind. Appl.*, vol. 51, no. 6, pp. 4372–4382, Nov. 2015.

[27] Y. Yang, N. Bianchi, C. Zhang, X. Zhu, H. Liu, and S. Zhang, "A method for evaluating the worst-case cogging torque under manufacturing uncertainties," *IEEE Trans. Energy Convers.*, vol. 35, no. 4, pp. 1837–1848, Dec. 2020.

[28] D. Xiang, Z. Q. Zhu, Y. H. Wu, F. Xu, and Y. F. Cheng, "Influence of magnet tolerances and rotor eccentricities on cogging torque of 12-slot/10-pole PM machines," in *Proc. 2nd Int. Conf. Sustain. Mobility Appl., Renewables Technol. (SMART)*, Nov. 2022, pp. 1–15.

[29] Y. Yang, N. Bianchi, G. Bramerdorfer, C. Zhang, and S. Zhang, "Methods to improve the cogging torque robustness under manufacturing tolerances for the permanent magnet synchronous machine," *IEEE Trans. Energy Convers.*, vol. 36, no. 3, pp. 2152–2162, Sep. 2021.

[30] D. Xiang and Z. Q. Zhu, "Influence of slot and pole number combinations on cogging torque in PM machines with tooth bulge and rotor eccentricity," in *Proc. 25th Int. Conf. Electr. Mach. Syst. (ICEMS)*, Nov. 2022, pp. 1–6.

[31] J. Wu, X. Zhu, D. Fan, Z. Xiang, L. Xu, and L. Quan, "A robust optimization design approach for hybrid PM machine considering asymmetric uncertainties of PMs," *IEEE Trans. Magn.*, vol. 58, no. 8, pp. 1–7, Aug. 2022.

[32] S. A. Evans, "Salient pole shoe shapes of interior permanent magnet synchronous machines," in *Proc. 19th Int. Conf. Electr. Mach. (ICEM)*, Sep. 2010, pp. 1–6.

[33] S. M. Hwang, J. B. Eom, Y. H. Jung, D. W. Lee, and B. S. Kang, "Various design techniques to reduce cogging torque by controlling energy variation in permanent magnet motors," *IEEE Trans. Magn.*, vol. 37, no. 4, pp. 2806–2809, Jul. 2001.

[34] X. Zhu, W. Hua, and G. Zhang, "Analysis and reduction of cogging torque for flux-switching permanent magnet machines," *IEEE Trans. Ind. Appl.*, vol. 55, no. 6, pp. 5854–5864, Nov. 2019.

[35] M. S. Mirazimi and A. Kiyoumarsi, "Magnetic field analysis of multi-flux-barrier interior permanent-magnet motors through conformal mapping," *IEEE Trans. Magn.*, vol. 53, no. 12, pp. 1–12, Dec. 2017.

[36] Z. Q. Zhu and D. Howe, "Instantaneous magnetic field distribution in brushless permanent magnet DC motors—III. Effect of stator slotting," *IEEE Trans. Magn.*, vol. 29, no. 1, pp. 143–151, Jan. 1993.

[37] L. R. Huang, J. H. Feng, S. Y. Guo, J. X. Shi, W. Q. Chu, and Z. Q. Zhu, "Analysis of torque production in variable flux reluctance machines," *IEEE Trans. Energy Convers.*, vol. 32, no. 4, pp. 1297–1308, Dec. 2017.

[38] C. S. Koh and J.-S. Seol, "New cogging-torque reduction method for brushless permanent-magnet motors," *IEEE Trans. Magn.*, vol. 39, no. 6, pp. 3503–3506, Nov. 2003.

[39] G. H. Kang, Y. D. Son, G. T. Kim, and J. Hur, "A novel cogging torque reduction method for interior-type permanent-magnet motor," *IEEE Trans. Ind. Appl.*, vol. 45, no. 1, pp. 161–167, Jan. 2009.

[40] E. Carraro and N. Bianchi, "Design and comparison of interior permanent magnet synchronous motors with non-uniform airgap and conventional rotor for electric vehicle applications," *IET Electr. Power Appl.*, vol. 8, no. 6, pp. 240–249, Jul. 2014.

YONGXI YANG received the B.Eng. and Ph.D. degrees in vehicle engineering from the Beijing Institute of Technology, Beijing, China, in 2014 and 2021, respectively.

He is currently a Postdoctoral Researcher of electrical engineering with the Harbin University of Science and Technology. His current research interest includes the robust design and optimization of PM machines with considerations of the effects of manufacturing tolerances.

WILLIAM CAI received the B.E. and M.E. degrees in electrical engineering from the Harbin University of Science and Technology, Harbin, China, in 1982 and 1985, respectively, and the Ph.D. degree in electrical and computer engineering from Clarkson University, Potsdam, NY, USA, in 1999.

He is currently a Professor with the Harbin University of Science and Technology. His current research interests include drive motors, power electronic controllers and automotive electric drive systems, rare earth permanent magnet motors, and new energy motor systems.

XIN JIN received the B.Eng. degree from Northeast Forestry University, in 2014, and the Ph.D. degree in vehicle engineering from the Beijing Institute of Technology, Beijing, China, in 2020.

He is currently a Researcher with the Beijing Institute of Space Launch Technology, China. His current research interests include electric vehicles, vehicular electric motor drive systems, and battery management systems.

SHUO ZHANG (Member, IEEE) received the B.Eng. degree from the North China Institute of Aerospace Engineering, Hebei, China, in 2011, and the Ph.D. degree in vehicle engineering from the Beijing Institute of Technology, Beijing, China, in 2017.

He is currently an Associate Professor with the National Engineering Laboratory for Electric Vehicles and the School of Mechanical Engineering, Beijing Institute of Technology. His current research interests include the modeling and control for the permanent magnet synchronous motor and hybrid power systems.

CHENGNING ZHANG received the M.E. degree in control theory and control engineering and the Ph.D. degree in vehicle engineering from the Beijing Institute of Technology, Beijing, China, in 1989 and 2001, respectively.

He is currently a Professor and the Vice Director of the National Engineering Laboratory for Electric Vehicles, Beijing Institute of Technology. His current research interests include electric vehicles and vehicular electric motor drive systems.

RUI LI received the M.E. degree in electrical engineering from the Harbin University of Science and Technology, Harbin, China.

He is currently the Director of the Machine Design Department, Harbin Electric Corporation Jiamusi Electric Machine Company Ltd. His current research interest includes electrical machine design and optimization.

YUE ZHAO received the bachelor's degree in vehicle engineering from Shijiazhuang Tiedao University, in 2018. He is currently pursuing the Ph.D. degree with the Beijing Institute of Technology.

His current research interests include robust design and optimization on electrical machines and cogging torque analysis considering manufacturing tolerances.